Low-temperature synthesis and characterization of lead-free BaTi0.89Sn0.11O3 piezoelectric powders

Marwa Zahid, Ouissal Kharraz, M'barek Amjoud, Daoud Mezzane, Mohamed Gouné, Khalid Hoummada, Ismael Saadoune, Sébastien Fourcade, Pierre Stocker, Brigita Rožič, et al.

Low-temperature synthesis and characterization of lead-free $BaTi_{0.89}Sn_{0.11}O_3$ piezoelectric powders

Marwa Zahid[1*], Ouissal Kharraz[1], M'barek Amjoud[1], Daoud Mezzane[1,2], Mohamed Gouné[3], Khalid Hoummada[4], Ismael Saadoune[1],Sebastien Fourcade[3], Pierre Stocker[5], Brigita Rožič[6] and Zdravko Kutnjak[6] and Mimoun El Marssi[2]

1. *IMED-Lab, Cadi-Ayyad University, FST, Marrakech, 40000, Morocco,*
2. *LPMC, University of Picardie Jules Verne, Amiens, 80039, France,*
3. *ICMCB, University of Bordeaux, Pessac, 33600, France,*
4. *IM2NP, Aix Marseille University, Marseille, 13397, France,*
5. *Aix Marseille Univ, CNRS, ICR, UMR 7273, SMBSO, Marseille, 13013, France,*
6. *Jožef Stefan Institute, Jamova Cesta 39, Ljubljana, 1000, Slovenia.*

Abstract:

Barium stannate titanate ($BaTi_{0.89}Sn_{0.11}O_3$, BTS_{11}) is one of the reported lead-free materials that exhibits high dielectric and piezoelectric properties near ambient temperature. In this work, BTS_{11} powders were elaborated via a soft chemistry method at very low temperatures using two synthesized approaches combining sol-gel and hydrothermal processes. In the first approach, the effect of the barium precursor on the purity and the crystallinity of the BTS_{11} powders was studied, while in the second approach, the influence of the hydrothermal temperature on the BTS_{11} proprieties was analyzed. Pure and uniform fine powders were obtained at 180°C, the appropriate mass fraction of BTS_{11} which leads to high suspension stability in water is below 3%. These eco-friendly and pure piezoelectric powders can be used without further heat-treatment in several applications such as lead-free piezoelectric decontamination of organic pollutants and photocatalyst, hydrogen generation and as fillers in flexible nanocomposites nano-generators for energy harvesting and energy storage.

Key words: Lead-free piezoelectric, barium stannate titanate, sol-gel, hydrothermal, low-temperature chemistry.

1. Introduction :

Lead-based perovskite materials have been considered the best candidate for energy storage, energy harvesting, piezoelectric photo-degradation and hydrogen production applications, owing to their unrivalled dielectric properties. However, due to the lead toxicity, and the strict limitation of its usage, replacing it with an eco-friendly material became an urgent and legitimate task. For this purpose, barium titanate ($BaTiO_3$, abbreviated as BT) is regarded as one of the potentially promising lead-free ceramics alternatives. However, due to its low dielectric constant, high curie temperature (120 °C) and narrow temperature stability, researchers have enhanced its properties by site-doping, hence many barium titanate systems have been studied over the years, such as BCZT [1], BST [2], BCTS [3],[4], and finally BTS or barium stannate titanate[5].

* Corresponding author.
*E-mail address:*marwa.zahid@ced.edu.ma

It was reported that replacing titanium ions with tin ions shifts the Curie temperature (T_c) toward lower values. When Tin content is about 11%, a quasi-quadruple point (with coexisting cubic, tetragonal, orthorhombic and rhombohedral phases) that exhibits double morphotropic phase boundaries coexist together near the ambient temperature, leading to high dielectric constant, high piezoelectric coefficient, and therefore enhanced energy storage[5]. Moreover, Yong gang Yao et al. obtained the highest piezoelectric coefficient d_{33} of 697pC/N, five times higher than that of pure $BaTiO_3$, in $BaTi_{0.89}Sn_{0.11}O_3$ in the vicinity of two converged triple points with coexisting multi-phase [6]. Meanwhile, Kalyani et al. showed that Sn substitution at low concentration drastically increased the piezoelectric coefficientd_{33} from 190 to 425 pC/N comparable to that exhibited by lead-zirconate titanate (PZT) [7].Barium stannate titanate was mainly studied in the bulk ceramics elaborated by a conventional solid-state reaction [5],[8],[9], or in the thin films using a sol-gel solution [9,10]. However, very few researchers highlighted BTS powders elaborated at low temperatures and their potential applications as fillers in organic polymers to enhance the energy storage and the energy harvesting in nano-generators for energy harvesting and motion-sensing [10], or as BTS_{11} nanoparticles for high dyes degradation and hydrogen generation efficiency [11].

The present work provides a detailed study on structural and physicochemical properties of ($BaTi_{0,89}Sn_{0,11}O_3$, BTS_{11}) powders synthesized by a combined Sol-Gel/Hydrothermal method at very low temperatures using two approaches which combine the advantages of excellent homogeneity, high purity, and low reaction temperature over other synthesis methods.

2. Experimental details:

2.1. Chemicals:

In order to prepare the BTS_{11} ceramics, barium acetate $Ba(CH_3COO)_2$ 99%, barium chloride ($BaCl_2$) 99.99%, barium hydroxide ($Ba(OH)_2$) 98.8%, titanium isopropoxide ($C_{12}H_{28}O_4Ti$) 97%, and tin chloride ($SnCl_2.2H_2O$) 98%, were used as raw materials, whereas acetic acid and 2-Methoxyethanol were used as the solvents. All reagents and solvents of chemical grade were used without any further purification.

2.2. Preparation of BTS_{11} powders

The $BaTi_{0,89}Sn_{0,11}O_3$ (here after called as BTS_{11}) powders were elaborated according to two synthesized approaches. The first one involves the study of the influence of three barium precursors on the purity and microstructure of the BTS_{11} powders since it is mostly the primary source of impurities in low-temperature synthesis, and in the hydrothermal process more specifically [12],[13]. The three considered barium precursors have the distillated water as the common solvent which instantly leads to the titanium precursor (titanium isopropoxide) hydrolysis, thus, the necessity to separate the A site (Barium) from the B site (Tin and Titanium) of the perovskite as described in the first approach's experimental section. The second approach highlighted the effect of the hydrothermal temperature ranging from room temperature to 180 °C by using the adequate barium precursor (barium acetate) selected in the first approach. In order to reach a better homogeneity and to avoid any intermediates products, all precursors were mixed together in a separate sol-gel step to form a BTS_{11} precursor in this approach. The concentration of the NaOH was fixed to 10M in both approaches.

The NaOH concentration has been previously studied by Xiang Ji et al. in BCZT perovskite powders, and they deduced that the higher NaOH concentration, the higher the cristallinity and the better

homogeneity, they also found that the grain size decreases with the increase of the NaOH concentration [14]. Furthermore, Z. hannani et al. also used NaOH 10M to elaborate BCZT perovskite powders and achieved high cristallinity [1].

2.1a First approach: effect of barium precursor type

An appropriate amount of titanium isopropoxide and tin chloride were mixed in isopropanol under an inert atmosphere (N_2) and stirred continuously until a homogenous mixture was achieved in one hour. Drops of distilled water were added to obtain the gel precursor. The gel precursor was then dried overnight at 80 °C. Next, the obtained precursor powder was homogeneously dispersed in 70 ml of 10M NaOH solution and mixed with a solution of barium acetate, barium chloride or barium hydroxide dissolved in 50ml of distilled water in a round-bottom flask with a magnetic stirrer for 3 hours under nitrogen flow. After that, the obtained suspension was poured in a Teflon stainless-steel autoclave at 180°C in an oven for 24h. Finally, the resulting BTS_{11} powders were washed with distilled water and ethanol several times and dried at 80°C for 12 hours without of any calcinations.

2.1b Second approach: effect of hydrothermal temperature

In the second approach, an appropriate amount of the adequate precursor (barium acetate) was dissolved, under stirring at 40°C for 1 hour, in acetic acid instead of water to avoid the hydrolysis of tin and titanium precursors. At the same time, in a beaker, a stoichiometric ratio of tin chloride and titanium isopropoxide were added to 2-propanol under continuous stirring and flow of nitrogen gas. The two solutions were then mixed in a 100ml flat bottom flask and left stirring for 2 hours; ammonia was then added until the solution turned clear by adjusting the pH at 7. The resulted gel was then dried overnight at 80 °C to form a white powder that was then dispersed in a 10M NaOH solution for 45 minutes, and then the suspension was transferred to a Teflon-lined stainless-steel autoclave, sealed and heated at 25, 80, 130 and 180 °C for 24 h. The main goal was to achieve a crystalline and pure perovskite powders at the lowest possible temperature, so we started at room temperature (25 °C) and gradually increased the temperature by 50 °C until we reached the purest crystalline ceramic powder at 180 °C. Finally, the resulting BTS_{11} powders were washed with distilled water and ethanol several times and dried at 80 °C for 12 hours without the need of any calcinations.

3. Characterizations

XRD measurements were carried out using an X-ray diffractometer brand "RIGAKU". X-rays were produced from a CuKα radiation source, having a wavelength equal to 1.54056 Å. X-ray diffraction spectra were recorded at room temperature in the range of 2θ between 20° and 80° with angle steps of 0.02°. The scanning speed of 5°/min was employed to perform simple phase identification. The scanning electron microscopy SEM observations were performed to examine our powders' morphology and approximate grain sizeona“Tescan Vega3” microscope. Moreover, in order to have a quick insight on the purity of our samples, the FTIR measurements have been carried out using a Bruker Vertex 70 spectrophotometer in transmission mode, 0.001 g of the powders were dispersed in 0.099 g of KBr matrix and analyzed in the frequency range 400 - 4000 cm^{-1}.The combined thermogravimetric and differential thermal analyses (TG-DTA,Sytram LABSYS Evo) were also performed at a heating rate of 5 ℃/min from room temperature to 700 ℃ in air. Differential scanning calorimetry

(Perkin Elmer Jade DSC) was used to point out the different phase transitions in a temperature range of 0 to 90 °C.A NanoSp confotec-MR520 was used in order to perform the Raman spectroscopy, the samples were analyzed using a laser with a wavelength of 532 nm in a 1200 line/mm network, and lastly, a NanoZs, Malvern instruments Ltd, 7.12 was used for our zeta potential measurements at T = 25 °C with the switch time at t = 60 s.

4. Results and discussion:

4.1. First approach: selection of barium precursor type

Fig.1 displays the XRD patterns of the BTS_{11} powders synthesized at 180 °C using the three Ba precursors according to the first approach; it is worth noting that all the three samples exhibit a perovskite structure with a notable difference in the purity. When using barium hydroxide as barium precursor, an intense peak around 2θ=21° corresponding to $BaSn(OH)_6$ impurity according to ICCD 15-780 is observed[15]. The presence of barium carbonate $BaCO_3$ as a secondary phase is observed when using barium chloride which could be attributed to the reaction between Ba^{2+}, and CO_2 wich originated from the decomposition of organic solvents and/or dissolved in the Ba precursor's solvent. $BaCO_3$ impurity can also occur as a byproduct due to atmospheric CO_2 contamination and the high thermodynamic stability of $BaCO_3$ at high pH in aqueous solution compared to $BaTiO_3$ [16]. Although, interestingly, no secondary phase was detected in the XRD patterns when the barium acetate was used as a precursor, which is confirmed by the FTIR spectra of the three sample presented infig.1, the vanishment of the peak around 1400 cm^{-1} and 1500 cm^{-1} corresponding to the carbonates is noticeable when the barium acetate was used. Hence the choice of the barium acetate as the barium precursor in the second approach, further characterizations were done to complete the study.

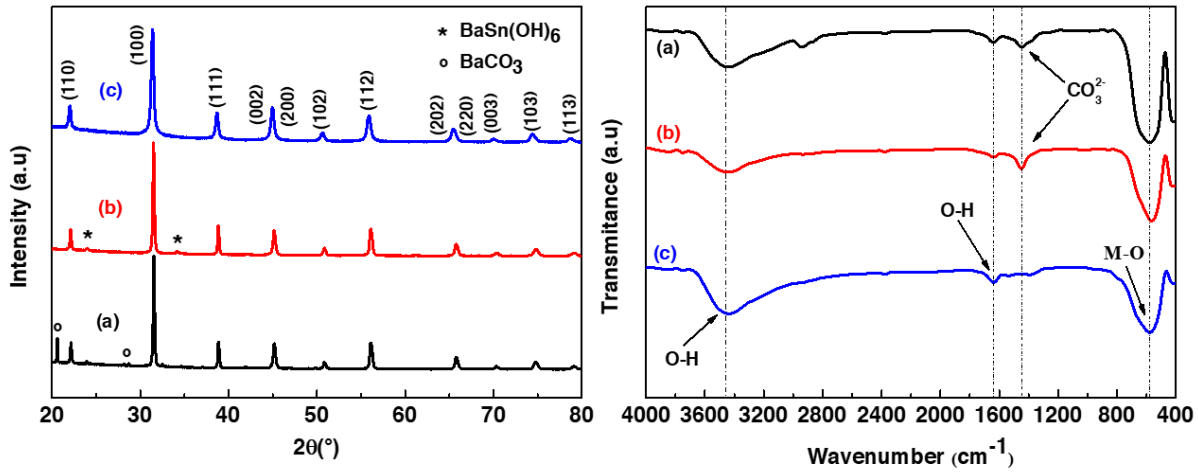

Fig.1 XRD patterns and FTIR spectra of the BTS_{11} powders synthesized at 180°C by the first approach (a) barium hydroxide (b) barium chloride (c) barium acetate.

4.2. Second approach: selection of hydrothermal temperature

In order to elucidate the effect of the hydrothermal temperature on the properties of BTS_{11} powders, barium acetate was used as the Ba precursor.

Fig.2 reveals the XRD patterns of BTS_{11} powders elaborated according to the second approach at different temperatures (25 °C, 80°C, 130 °C and 180 °C) with a scanning angle from 20° to 80°. It was observed that all

BTS_{11} powders exhibit a perovskite phase along with the one synthesized at room temperature. It is also worth noting that the presence of a very weak peak at 24° may correspond to $BaCO_3$ in the samples synthesized at 25 °C, 80 °C and 130 °C, which is due to the reaction of Ba^{2+} with CO_2 despite inert atmosphere usage. Selvaraj et al. [17] reported that $BaTiO_3$ (BT) nanopowders prepared by combining sol–gel and hydrothermal processes at various hydrothermal temperatures were found to be in crystalline nature along with impurities like barium carbonate ($BaCO_3$) and the intensity of diffraction peaks corresponding to $BaCO_3$ decreased with increasing temperature. However, at 180 °C, no secondary phases are detected, therefore the structure is highly pure. This demonstrates that the precursor powders synthesized by Sol-Gel is entirely transformed into well-crystallized BTS_{11} powder in the hydrothermal step which is also confirmed by the thermogravimetric analysis of the powder synthesized at 180 °C presented in the fig. 3-a. The total weight loss observed in temperature range of 30 °C - 700 °C is very low, 7% approximately. The first weight loss is due to the dehydration phenomena. It occurs at a temperature range of 40-160 °C. The second weight loss observed at 160 to 230 °C is ascribed to the chemical dehydroxylation and the decomposition of solvents, and the last low weight loss after 580 °C is associated to the thermal decomposition of remaining organic compounds [18].

The FTIR spectra of BTS_{11} powders synthesized at different temperatures were performed to study the purity of our powders more deeply as presented in fig.4. When the reaction temperatures are 25 °C and 80 °C, a weak absorption peak corresponding to CO_3^{2-} at around 862 cm^{-1} can be attributed to the few impurities of CO_3^{2-} that were also detected by XRD. With the temperature increase, the extremely weak absorption peak of CO_3^{2-} disappears. Moreover, the absorption peaks at 3000–3600 cm^{-1} (the symmetric and asymmetric stretching vibrations of O–H), 1633 cm^{-1} (the bending vibration of H–O–H) and 1421 cm^{-1} (the symmetric stretching of C=O) also decline gradually, indicating the improvement of the chemical purity of BTS_{11} powders. Finally, when the temperature approaches 180 °C, the intensity of the peaks corresponding to O–H and the C=O liaisons nearly disappear, indicating good purity of the obtained powders [19].

Multiphase such as rhombohedral (R,R3m), orthorhombic (O,Amm2), tetragonal (T, P4mm) and also cubic (C, Pm3m), were observed in the $BaTi_{0.89}Sn_{0.11}O_3$, system by many researchers[11],[20],[21],[22]. The splitting observed in the enlarged view of the 45° XRD peak (fig.2-e) suggests the presence of a tetragonal phase, while the presence of a triplet at 65° (fig.2-f) indicates the existence of an orthogonal phase as well [23],[24],[25]. Thus, to confirm these observations, full-pattern Rietveld refinement was performed and presented in fig.3. The presence of the tetragonal, orthorhombic and the rhombohedral was confirmed with a phase fraction of 55.77%, 18.59% and 25.64% respectively. The refinement parameters are presented in table.1.

The Differential scanning calorimetry (DSC) was performed on the sample synthesized at 180 °C as presented in fig.4-b. The presence of only one weak endothermic peak in a temperature range close to ambient temperature, between 30°C and 45°C implies the existence of a multiphase [18]. It is well known that a sudden change in spontaneous polarization during a first-order transition will produce latent heat and specific heat dissipation at the Curie temperature, meanwhile, the tricritical behavior refers to a special thermodynamic condition in which a first-order transition becomes a second-order transition, so due to the discontinuity of polarization, it involves a discontinuous change in specific heat, hence the transition can almost be undetectable and the intensity of the peak is much smaller from the first-order transition [26],[27]. Thus, the presence of one endothermic peak in a temperature range between 0°C and 90 °C, can leads that T_{R-O}, T_{O-T} and T_c are all overlapped in the temperature

range, between 30 °C and 45 °C. Therefore, high values of the dielectric constant and piezoelectric coefficient can be achieved in this temperature range due to the properties of the multiple phase boundaries [11],[21].

Raman spectroscopy is a versatile method to probe structural properties at the nanoscale and is often used to study structural transitions in ferroelectrics. Fig.4 shows Raman spectra at room temperature of BTS_{11} powders synthesized at 25 °C, 80 °C, 130 °C and 180 °C. The modes at 190 cm^{-1},253 cm^{-1}, 305 cm^{-1}, 513 cm^{-1} and 716 cm^{-1} corresponding to A_1(LO), A_1(TO), B_1,E(TO,LO), A_1(TO) and A_1,E(LO) respectively [28]. Raman peaks at around 305 and 716 cm^{-1}, characteristics bands of the ferroelectric phases, show weak peaks at low temperatures, and become more intense and sharper with increasing the synthesis temperature. Likewise, the intensity of the cubic paraelectric phase characterized by two peaks centered at 253 and 513 cm^{-1} is weak at low temperatures and well-defined at 180 °C, which also suggests the presence of multiphase. The Raman peak at 870 cm^{-1} is due to the B site vacancies originating from the incomplete substitution of tin in the barium titanate matrix. The peak disappears when the temperature exceeds 130 °C, suggesting a complete conversion of our raw materials into the perovskite structure [29]. It is worthy to note that when the synthesizing temperature increases, the characteristic peaks of the perovskite structure around 190, 305, 513 and 716 cm^{-1} are getting sharper, which implies that the crystalline quality of the BTS_{11} powder is improved, in perfect correlation with the XRD results analysis[28][30].

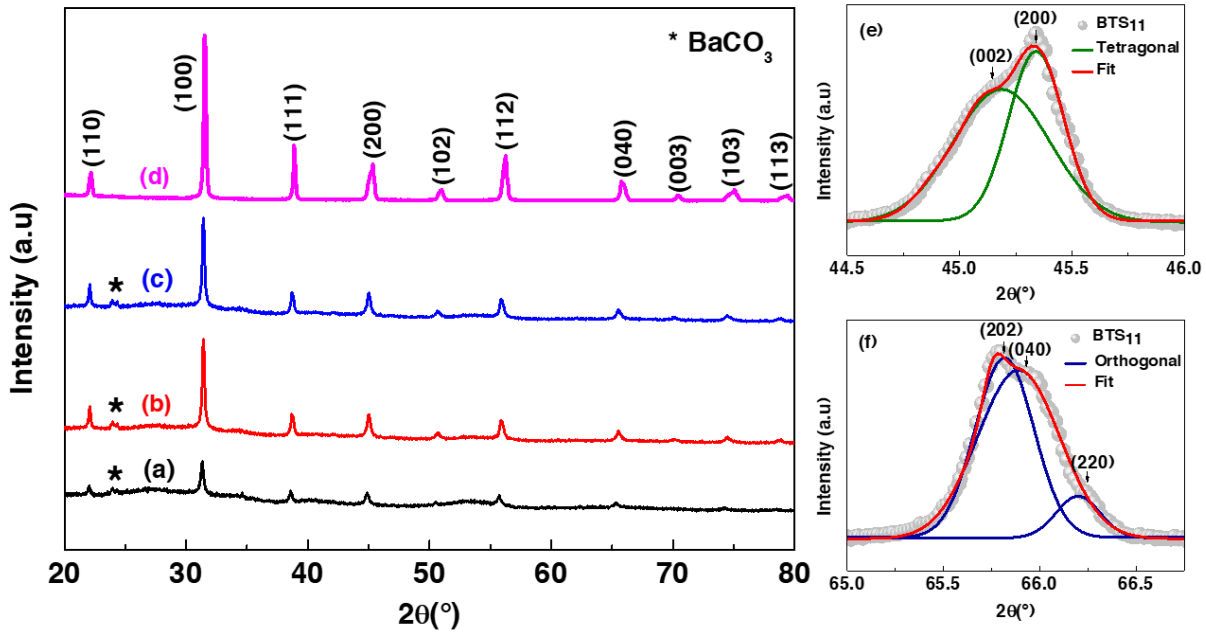

Fig.2XRD patterns of BTS_{11} powders synthesized at a) 25°C, b) 80°C, c)130°C and d)180°C and the enlarged views of 45° XRD peak (e) and 65° peak (f) of the BTS_{11} powder synthesized at 180 °C according to the second approach.

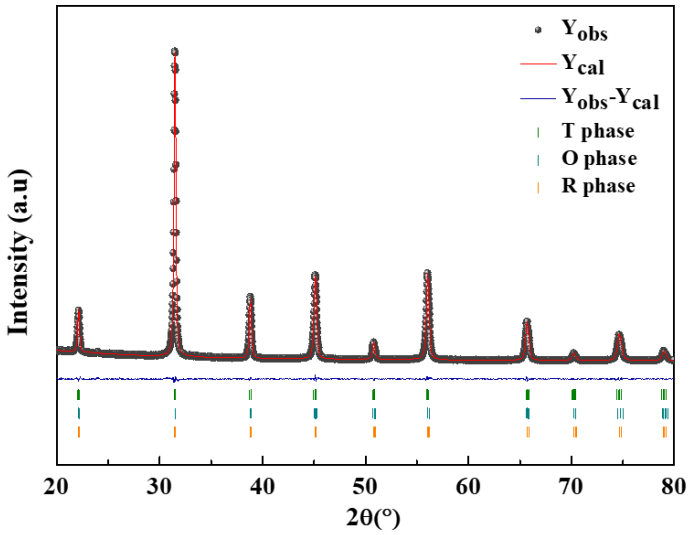

161

162 *Figure 3 Full pattern Rietveld refinement of the BTS_{11} particles synthesized at 180 °C*

163 **Table 1.** Refinement parameters of BTS_{11} by full pattern Rietveld refinements.

x	space group	a (Å)	b (Å)	c (Å)	α, β, γ (°)	Fraction (%)	GOF	R_{exp}	R_{wp}
0.11	*P4mm*	4.017506	4.017506	4.027725	90, 90, 90	55.77	1.4	5.49	7.73
	Amm2	4.017593	4.009575	4.023733	90, 90, 90	18.59			
	R3m	5.679052	5.679052	6.959726	90, 90, 120	25.64			

164

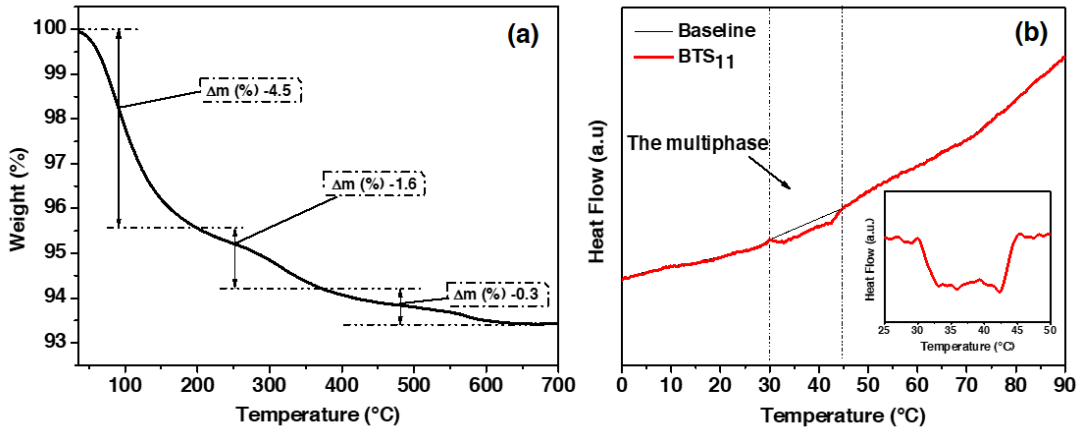

165

166 *Fig.4 (a) ATG curve and (b) DSC heat flow curve of the BTS_{11} powder synthesized by the second approach at 180°C(The inset*
167 *shows the zoom region from 25 to 50 °C).*

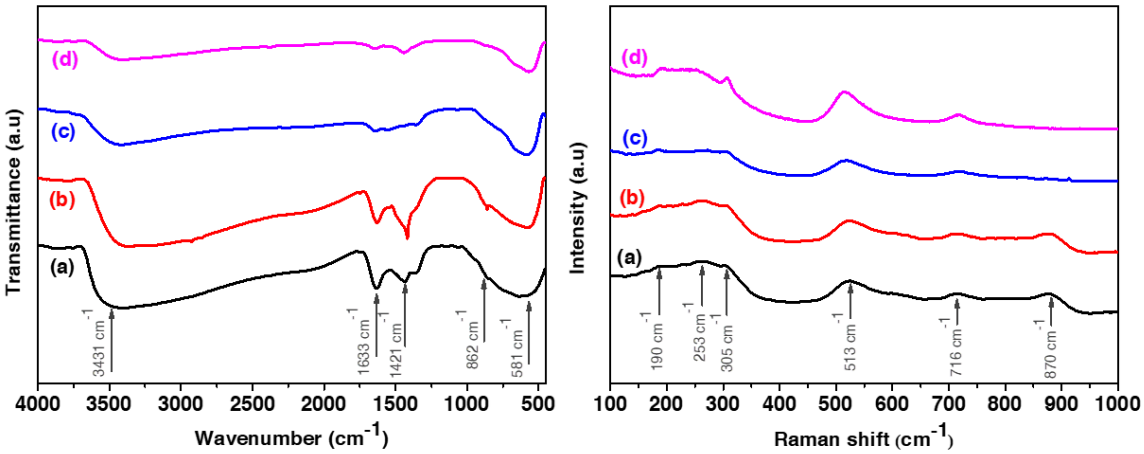

Fig.5 Raman and FTIR spectra of the BTS_{11} powders synthesized at a) 25 °C, b) 80 °C, c) 130 °C and d) 180 °C according to the second approach.

The SEM micrograph of the sample synthesized at 180 °C is shown in fig.5-a. The pure BTS_{11} powder synthesized at 180°C is spherically shaped and well homogenized with a distribution range of 475 nm.

To understand the surface charge of our powders and their electrostatic stabilization in a suspension during colloidal processing, zeta potential mesurements have been conducted in distilled water. The zeta potential of a particle in a solution is determined by the charges on the various parts of the particle, the amount of associated solvent and the ionic strength of the solution. The zeta potential is a measure of the strength of the intermolecular forces between the particle and the solvent, and it is a measure of the repulsive tendency of the associated solvent to the particle[31]. The larger the zeta potential, the stronger the associated intermolecular forces and the more difficult it is for a particle to slip or migrate through a solution[32]. If all particles in a suspension have a large negative or positive zeta potential ($|\xi| > 30$ mV), they will tend to repel each other and the particles will not clump together leading to a stable solution. However, if the particles have low zeta potential values ($|\xi| < 30$ mV), the repulsive force is not sufficient to prevent the particles from clumping together and flocculating [33]. Thus, itis crutial to control the surface chemical interactions between BTS_{11} particles and different additives, such as electroactive polymers and organic pollutants in different media where aqueous suspension are preferredowing to environmental considerations. The zeta potential of our as-prepared powders (1% in mass) measured immediately after the colloidal preparation (Fig.5-b) shows negative surface charges and decreases when the synthesis temperature increases starting from a value of -17.8 mV to -40.8 mV. However, when the temperature is above 130 °C, the zeta potential is higher in absolute value than 40 mV and the system isconsidered completely stable. These results are agree with FTIR analysis showing the decrease of the number of carbonate and hydroxyl groups remaining in the particles when the hydrothermal temperature increases.

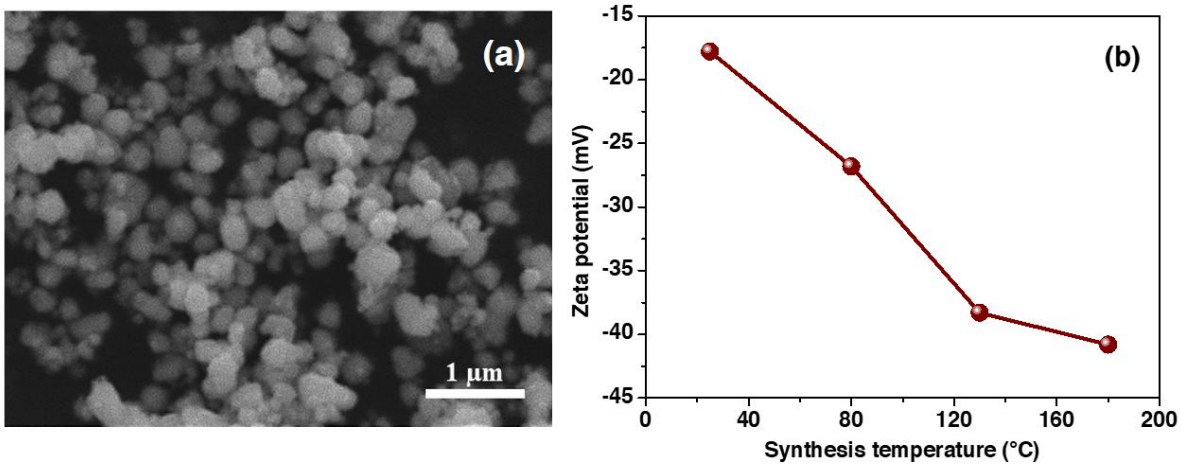

Fig.6 (a) SEM micrograph of the BTS_{11} powder synthesized according to the second approach at 180 °C and (b) Synthesis temperature dependent zeta potential.

The percentage of the filler in the organic polymer matrix is a critical parameter in the functional properties of the nanocomposites generators, such as the dielectric constant, breakdown strength and the energy storage density[34],[35],[36]. It was reported that high mass fraction of the filler, leads to higher dielectric constant but low breakdown strength[37].However, low fillers not only improves the breakdown strength of the nanocomposites, but also remarkably enhance their mechanical strength [38]. Thus, low mass fraction is advisable. Fig.6 represents the zeta potential of the BTS_{11} powder in distilled water using different mass fraction ranging from 1% to 5%to test the stability and the dispersibility of the particles. The result shows that above 3%, the zeta potential starts drastically increasing showing that the system become unstable due to the agglomeration of the particles[39], however when using a low filler fraction (less than 3%), the BTS_{11} exhibits high stability and dispersibility and no further surface modification is required. The highly negative zeta potential yielding to repulsive forces at the surface and a high degree of dispersibility and stability is found when the BTS_{11} mass fraction is 3%.

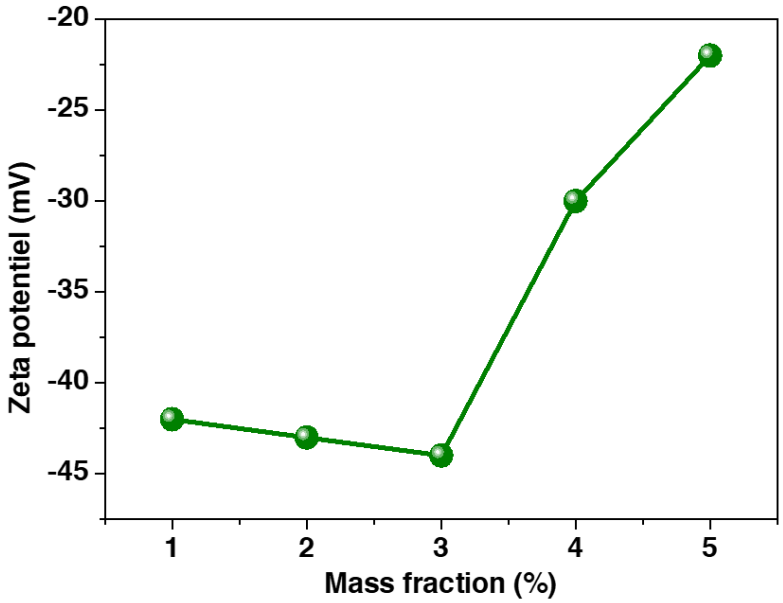

Fig.7 Mass fraction dependent Zeta potential of the BTS_{11} powder in distillated water synthesized according to the second approach.

So, it is worth noting that the BTS_{11}powder prepared at 180 °C, tend to be easily dispersed into water at low fraction and hence used as piezo-photocatalysis for dye decomposition and hydrogen production or as fillers in polymers nanocomposites for energy harvesting and energy storage. However, functionalizing the surface of the BTS_{11} particles is recommended when using a high filler fraction.

5. Conclusion:

Non-toxic and ecological $BaTi_{0.89}Sn_{0.11}O_3$ (BTS_{11}) powders were successfully prepared at very low temperature using sol-gel and hydrothermal methods combined without any further heat treatment. The effect of the barium precursor on the purity of the materials was studied. The hydrothermal synthesis temperature was proven to be a key factor for the crystalline purity of the powders and the improvement of their suspension stability. The mass fraction of 3% is the most suitable conditions for the BTS_{11} colloidal stability in the water. The Curie temperature of the powder was estimated to be around room temperature using the differential scanning calorimetry (DSC), which gives our eco-friendly powders huge advantages and potential applications as nanogenerators for energy storage, energy harvesting and hydrogen production and as piezoelectric photocatalysts.

Acknowledgments

The authors gratefully acknowledge the generous financial support of the European Union Horizon 2020 Research and Innovation actions MSCA-RISE-ENGIMA (No. 778072) and MSCA-RISE-MELON (No. 872631) and ARRS project J1-9147 and program P1-0125 and CNRST Priority Program PPR 15/2015 and the ministry of Science and Higher Education of the Russian Federation, grant agreement No 075-15-2021-953.

References:

[1] Z. Hanani, E.-H. Ablouh, M. ’barek Amjoud, D. Mezzane, S. Fourcade, M. Gouné, Ceram. Int. 44 (2018) 10997–11000.
[2] Y.J. Wu, J. Eur. Ceram. Soc. (2017) 6.
[3] H. Zaitouni, L. Hajji, D. Mezzane, E. Choukri, A. Alimoussa, S. Ben Moumen, B. Rožič, M. El Marssi, Z. Kutnjak, Phys. B Condens. Matter 566 (2019) 55–62.
[4] Y. Hadouch, S. Ben Moumen, H. Mezzourh, D. Mezzane, M. Amjoud, B. Asbani, A.G. Razumnaya, Y. Gagou, B. Rožič, Z. Kutnjak, M. El Marssi, J. Mater. Sci. Mater. Electron. (2022).
[5] L. Jin, Ceram. Int. (2018) 9.
[6] Y. Yao, C. Zhou, D. Lv, D. Wang, H. Wu, Y. Yang, X. Ren, EPL Europhys. Lett. 98 (2012) 27008.
[7] A.K. Kalyani, H. Krishnan, A. Sen, A. Senyshyn, R. Ranjan, Phys. Rev. B 91 (2015) 024101.
[8] K.C. Singh, J. Alloys Compd. (2011) 5.
[9] X. Wei, X. Yao, Mater. Sci. Eng. B (2007) 5.
[10] M.A. Al-Akhras, S. Saq’an, Z. Ghadieh, Acta Phys. Pol. A 130 (2016) 447–449.
[11] Q. Zhao, H. Xiao, G. Huangfu, Z. Zheng, J. Wang, F. Wang, Y. Guo, Nano Energy 85 (2021) 106028.
[12] M.Z.-C. Hu, V. Kurian, E.A. Payzant, C.J. Rawn, R.D. Hunt, Powder Technol. 110 (2000) 2–14.
[13] G.D. Webler, M.J.M. Zapata, G.S. Maciel, A. Patra, J.M. Hickmann, M.A.R.C. Alencar, J. Nanomater. 2014 (2014) 1–9.
[14] X. Ji, C. Wang, W. Luo, G. Chen, S. Zhang, R. Tu, Q. Shen, J. Shi, L. Zhang, J. Sol-Gel Sci. Technol. 94 (2020) 205–212.
[15] A. Marikutsa, M. Rumyantseva, A. Baranchikov, A. Gaskov, Materials 8 (2015) 6437–6454.
[16] M. del C.B. López, G. Fourlaris, B. Rand, F.L. Riley, J. Am. Ceram. Soc. 82 (1999) 1777–1786.
[17] M. Selvaraj, V. Venkatachalapathy, J. Mayandi, S. Karazhanov, J.M. Pearce, AIP Adv. 5 (2015) 117119.
[18] Z. Hanani, S. Merselmiz, A. Danine, N. Stein, D. Mezzane, M. Amjoud, M. Lahcini, Y. Gagou, M. Spreitzer, D. Vengust, Z. Kutnjak, M. El Marssi, I.A. Luk’yanchuk, M. Gouné, J. Adv. Ceram. 9 (2020) 210–219.
[19] X. Jin, D. Sun, M. Zhang, Y. Zhu, J. Qian, J. Electroceramics 22 (2009) 285–290.
[20] M. Zahid, Y. Hadouch, M. Amjoud, D. Mezzane, M. Gouné, K. Hoummada, A. Alimoussa, A.G. Razumnaya, B. Rožič, Z. Kutnjak, J. Mater. Sci. Mater. Electron. (2022).
[21] J. Gao, Y. Wang, Y. Liu, X. Hu, X. Ke, L. Zhong, Y. He, X. Ren, Sci. Rep. 7 (2017) 40916.
[22] S. Merselmiz, Z. Hanani, D. Mezzane, M. Spreitzer, A. Bradeško, D. Fabijan, D. Vengust, M. Amjoud, L. Hajji, Z. Abkhar, A.G. Razumnaya, B. Rožič, I.A. Luk’yanchuk, Z. Kutnjak, Ceram. Int. 46 (2020) 23867–23876.
[23] G.K. Sahoo, R. Mazumder, J. Mater. Sci. Mater. Electron. 25 (2014) 3515–3519.
[24] D.S. Keeble, F. Benabdallah, P.A. Thomas, M. Maglione, J. Kreisel, Appl. Phys. Lett. 102 (2013) 092903.
[25] Z. Hanani, D. Mezzane, M. Amjoud, A.G. Razumnaya, S. Fourcade, Y. Gagou, K. Hoummada, M. El Marssi, M. Gouné, J. Mater. Sci. Mater. Electron. 30 (2019) 6430–6438.
[26] J. Gao, Y. Wang, Y. Liu, X. Hu, X. Ke, L. Zhong, Y. He, X. Ren, Sci. Rep. 7 (2017) 40916.
[27] O.R. Ghita, M.A. Beard, J. McCabe, R. Bottom, J. Richmond, K.E. Evans, J. Mater. Sci. 43 (2008) 4988–4995.

[28] L. Veselinović, M. Mitrić, L. Mančić, M. Vukomanović, B. Hadžić, S. Marković, D. Uskoković, J. Appl. Crystallogr. 47 (2014) 999–1007.
[29] V.K. Veerapandiyan, S. Khosravi H, G. Canu, A. Feteira, V. Buscaglia, K. Reichmann, M. Deluca, J. Eur. Ceram. Soc. 40 (2020) 4684–4688.
[30] P. Ren, Z. Liu, Q. Wang, B. Peng, S. Ke, H. Fan, G. Zhao, Sci. Rep. 7 (2017) 6693.
[31] K. Suttiponparnit, J. Jiang, M. Sahu, S. Suvachittanont, T. Charinpanitkul, P. Biswas, Nanoscale Res Lett 6 (2011) 27.
[32] M. Larsson, A. Hill, J. Duffy, (n.d.) 7.
[33] S. Wu, D. Zhu, X. Li, H. Li, J. Lei, Thermochim. Acta 483 (2009) 73–77.
[34] K.B. Nilagiri Balasubramanian, T. Ramesh, Polym. Adv. Technol. 29 (2018) 1568–1585.
[35] Y. Dang, Y. Wang, Y. Deng, M. Li, Y. Zhang, Z. Zhang, Prog. Nat. Sci. Mater. Int. 21 (2011) 216–220.
[36] S.F. Mendes, C.M. Costa, C. Caparros, V. Sencadas, S. Lanceros-Méndez, J. Mater. Sci. 47 (2012) 1378–1388.
[37] S. Liu, S. Xue, W. Zhang, J. Zhai, G. Chen, J Mater Chem A 2 (2014) 18040–18046.
[38] T. Hassan, A. Salam, A. Khan, S.U. Khan, H. Khanzada, M. Wasim, M.Q. Khan, I.S. Kim, J. Polym. Res. 28 (2021) 36.
[39] R.H. Huang, N.B. Sobol, A. Younes, T. Mamun, J.S. Lewis, R.V. Ulijn, S. O'Brien, ACS Appl. Mater. Interfaces 12 (2020) 51135–51147.